

Polariton luminescence of mixed modes in crystals with spatial dispersion

A. G. Abukadyrov, M. I. Sazhin, A. V. Sel'kin, and N. Kh. Yuldashev

A. F. Yoffe Physico-Technical Institute, USSR Academy of Sciences

(Submitted 12 September 1989)

Zh. Eksp. Teor. Fiz. **97**, 644–662 (February 1990)

For the first time, certain peculiarities in the shape of the polariton luminescence (PL) spectra of anisotropic crystals have been investigated under conditions where the dissipative decay of excitons violates the criterion of applicability of the Boltzmann kinetic equation. We develop a theory of mixed-mode PL which takes into account spatial dispersion, and which is valid for arbitrary ratios of the real and imaginary parts of the radiating-state wave vectors. Using a mixed-mode emission geometry, we carried out low-temperature (2 K) measurements of the PL spectrum of CdS, recording the photoluminescence in various directions with respect to the normal to the radiating facet of the crystal. Using the results of our theoretical calculations, we can accurately reproduce all of our experimental data by treating the effective spatial decay length of the polariton distribution, the only quantity whose variation significantly affects the results, as an adjustable parameter. We have observed an effect associated with interference between radiating mixed-mode states, which is caused by elastic scattering of the polaritons in the spatially dispersive medium.

I. INTRODUCTION

Many features of the emission spectrum of crystals observed experimentally in the neighborhood of resonant frequencies associated with dipole-active optical transitions to exciton states can be described accurately by invoking the polariton luminescence mechanism¹⁻³ (see also Ref. 4 and the references cited therein). Within the formalism of the polariton approach, luminescence is a process in which polaritons lying on various dispersion-relation branches β with frequencies $\omega_\beta(\mathbf{K})$ are transformed at the crystal boundary into external photons with frequency $\omega = ck_0 = \omega_\beta(\mathbf{K})$, where c and k_0 are the velocity and wave vector of a photon in the external medium and \mathbf{K} is the polariton wave vector. This implies that the form of the luminescence spectrum will be determined by the spatial-energy distribution function of the polaritons and the conditions for transmission of radiation through the crystal surface.

As a rule, finding the distribution function involves solving the Boltzmann kinetic equation. If the angular dependence of the polariton scattering probability varies smoothly, the condition for applicability of the kinetic equation reduces to fulfillment of the following inequalities⁵:

$$|\operatorname{Re} \mathbf{K}_\beta| \gg \alpha_\beta \sim |\operatorname{Im} \mathbf{K}_\beta|, \quad (1)$$

$$|\operatorname{Re}(\mathbf{K}_{\beta'} - \mathbf{K}_{\beta''})| \gg \alpha_{\beta'}, \alpha_{\beta''}, \quad (2)$$

where $\beta' \neq \beta''$, and α_η are the absorption coefficients for polaritons on the dispersion branches $\eta = \beta, \beta', \beta''$. The first inequality implies that the mean free path of the polariton

$$l_\beta = \alpha_\beta^{-1} = v_\beta / \Gamma_\beta S_\beta$$

must exceed the wavelength

$$\lambda_\beta = 2\pi / |\operatorname{Re} \mathbf{K}_\beta|$$

(where $v_\beta = |d\omega_\beta/d\mathbf{K}_\beta|$ is the group velocity, Γ_β is the total inverse lifetime (i.e., the attenuation), and S_β is the oscillator strength¹ of the polariton on branch β). The second inequality corresponds to the condition that there be no

interference between polariton states on different dispersion branches. This interference arises for $\Gamma_\beta \neq 0$ and makes itself felt through additional interference currents in the energy.⁶

In principle, inequalities (1) and (2) can be made to hold by choosing crystals with sufficiently large longitudinal-transverse splitting ω_{LT} of the exciton state and sufficiently small values of Γ_β . However, under real conditions the inequalities (1) and (2) are often not fulfilled [particularly Eq. (1), when $\operatorname{Re} \mathbf{K}_\beta \rightarrow 0$], due to either the presence of permanent defects and impurities in the samples or to elevated crystal temperatures. In this situation, the problem of radiation transfer in the exciton region of the spectrum cannot be treated within the framework of the kinetic-equation approximation, and the question of how the polariton luminescence (PL) is generated in the presence of attenuation requires a special discussion.

From the point of view of experimental study of the situation, we found it extremely convenient to analyze the PL spectrum in terms of the mixed modes which can be excited in uniaxial crystals.⁷⁻¹⁰ By choosing an appropriate geometry for recording the emission, and by varying the angle θ between the wave vector of the mixed mode and the optical axis of the crystal, we can vary the effective "longitudinal-transverse" splitting $\omega_{LT}^{\text{eff}}(\theta)$ of the exciton state⁹⁻¹² and thereby change the ratio $\Gamma_\beta / \omega_{LT}^{\text{eff}}$. For sufficiently large values of ω_{LT}^{eff} , we expect that inequalities (1) and (2) are satisfied over practically the whole spectral region within the longitudinal-transverse splitting. However, as $\omega_{LT}^{\text{eff}} \rightarrow 0$ (which can be achieved by varying θ) there certainly will be some region of the spectrum where conditions (1) and (2) are violated. In this case, the interesting possibility arises of passing in an experimentally simple way (i.e., by varying ω_{LT}^{eff}) from a situation where inequality (2) is fulfilled to a situation where it is violated. The variability of ω_{LT}^{eff} allows us to investigate in detail the little-studied intermediate case between strong and weak exciton-phonon coupling, and also to create conditions under which spatial dispersion (SD)

gradually passes to anomalous dispersion.

In this paper we study the PL of mixed modes of uniaxial crystals both experimentally and theoretically under conditions such that inequalities (1), (2) are violated. A theory of PL is developed which is valid for arbitrary ratios of the real and imaginary parts of the wave vectors of the emitting states of the crystal, which are excited by scattering from polariton initial states with well-defined quantum numbers \mathbf{K} . The results of our theoretical calculations agree with the experimental PL spectrum of CdS crystals.

In Chapter II of this paper, we formulate the statement of the problem and expound on the method of calculating the PL spectrum of mixed modes for the case when it is necessary to go outside the framework of the kinetic approximation. In Chapter III we describe the basic details of the experiment and cite the experimental data on low-temperature PL of cadmium sulfide crystals in the geometry appropriate to the study of the mixed modes. A quantitative comparison of the experimental spectra with the numerical calculations and a discussion of the results are given in Chapter IV.

II. THEORY

1. Statement of the problem

Let us discuss the energy spectrum of polaritons of a uniaxial crystal in the neighborhood of an isolated dipole-active exciton state; we will assume that optical transitions into this state are allowed only for the optical polarization $\mathbf{E} \perp \mathbf{C}$, where \mathbf{C} is the optical axis of the crystal. The distinctive feature of such a spectrum, as is well known,¹³ is its strong anisotropy: for wave propagation in an arbitrary direction which differs from $\mathbf{K} \parallel \mathbf{C}$ and $\mathbf{K} \perp \mathbf{C}$, two transverse modes ($T1, T2$) and two modes of mixed type ($M1, M2$) can be excited at a fixed frequency (Fig. 1).

For a crystal with spatial dispersion, the dielectric permittivity tensor $\varepsilon_{ij}(\omega, \mathbf{K})$ of interest to us is characterized by only two components $\varepsilon_{\perp}(\omega, \mathbf{K})$ and $\varepsilon_{\parallel}(\omega, \mathbf{K})$, corresponding to the optical polarizations $\mathbf{E} \perp \mathbf{C}$ and $\mathbf{E} \parallel \mathbf{C}$, in the system of coordinates illustrated in the inset of Fig. 1. Near the resonance frequency we can assume $\varepsilon_{\parallel}(\omega, \mathbf{K}) \approx \varepsilon_{b\parallel} = \text{const}$, assume and that all the dependence of ε_{ij} on ω and \mathbf{K} is included in $\varepsilon_{\perp}(\omega, \mathbf{K})$ (see Ref. 8):

$$\varepsilon_{\perp}(\omega, \mathbf{K}) = \varepsilon_{b\perp} \left[1 + \frac{\omega_{LT}}{\omega_T(\mathbf{K}) - \omega - i\Gamma/2} \right], \quad (3)$$

where

$$\omega_T(\mathbf{K}) = \omega_0 + \hbar K_x^2 / 2M_{\parallel} + \hbar (\mathbf{K}^2 - K_x^2) / 2M_{\perp}, \quad (4)$$

while $\varepsilon_{b\perp}$ is the component of the background dielectric permittivity tensor for the polarization $\mathbf{E} \perp \mathbf{C}$, $\omega_{LT} = \omega_L - \omega_0$ is the longitudinal-transverse splitting, $\hbar\omega_0$ and $\hbar\omega_L$ are the minimum energies of the transverse and longitudinal exciton bands, K_x is the projection of the vector \mathbf{K} on the \mathbf{C} -axis, and M_{\perp}^{-1} and M_{\parallel}^{-1} are components of the inverse effective mass tensor of an exciton for the propagation directions $\mathbf{K} \perp \mathbf{C}$ and $\mathbf{K} \parallel \mathbf{C}$.

In the notation of (3) and in what follows, we will assume that the inequalities

$$\omega_{LT}, |\omega - \omega_0| \ll \omega_0$$

hold; this assumption is valid for many semiconductor crystals in common use within the spectral region of resonance exciton luminescence. Taking these inequalities into account, the dispersion relations for the modes under discussion are

$$c^2 \mathbf{K}^2 / \omega^2 = \varepsilon_{\perp}(\omega, \mathbf{K}) \quad (\text{modes } T1, T2),$$

$$\frac{c^2 K_x^2}{\omega^2 - c^2 (\mathbf{K}^2 - K_x^2) / \varepsilon_{\parallel}(\omega, \mathbf{K})} = \varepsilon_{\perp}(\omega, \mathbf{K}) \quad (\text{modes } M1, M2)$$

Taking (3) into account, we can write these relations in the form of functions $\omega(\mathbf{K})$:

$$\omega = \omega_{\mathbf{K}}^{(T)} \equiv \omega_T(\mathbf{K}) - \frac{\varepsilon_b \omega_{LT}}{(c\mathbf{K}/\omega_0)^2 - \varepsilon_b}, \quad (5)$$

$$\omega = \omega_{\mathbf{K}}^{(M)} \equiv \omega_M(\mathbf{K}) - \frac{\varepsilon_b \bar{\omega}_{LT}}{(c\mathbf{K}/\omega_0)^2 - \varepsilon_b}, \quad (6)$$

where

$$\begin{aligned} \omega_M(\mathbf{K}) &= \omega_T(\mathbf{K}) + \omega_{LT}, \\ \bar{\omega}_{LT} &= \omega_{LT} K_x^2 / (\varepsilon_b k_0^2) \end{aligned} \quad (7)$$

and $\varepsilon_b = \varepsilon_{b\perp} \approx \varepsilon_{\parallel}$.

The dispersion curves of the polariton upper branches (PUB) $T2$ and $M2$ shown in Fig. 1 are given by Eqs. (5), (6) in the region of wave vectors $|\mathbf{K}| < \varepsilon_b^{1/2} k_0$ as $\Gamma \rightarrow 0$; the curves $T1$ and $M1$ for the polariton lower branches (PLB) are given by these expressions for $|\mathbf{K}| > \varepsilon_b^{1/2} k_0$. For real frequency ω , there are solutions to Eqs. (5), (6) for which the wave vectors \mathbf{K} are complex, even for $\Gamma = 0$; these solutions correspond to surface radiating modes with $\text{Re } \mathbf{K}^2 < 0$ and $\text{Im } \mathbf{K}^2 = 0$ (i.e., $\text{Re } \mathbf{K} \cdot \text{Im } \mathbf{K} = 0$), which are excited at the crys-

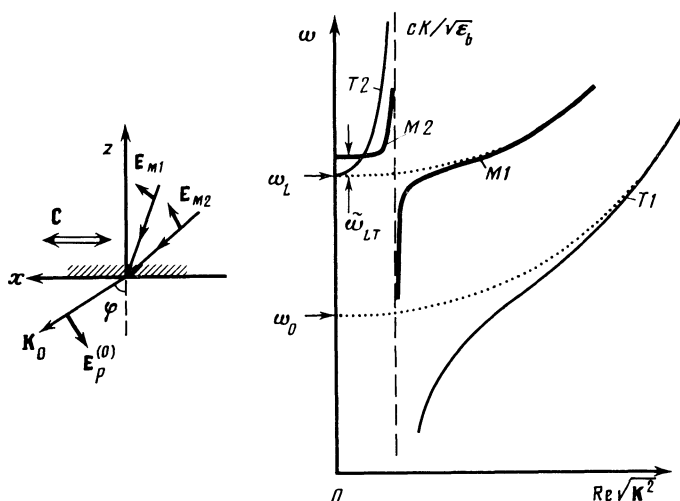


FIG. 1 Schematic illustration of the dispersion curves for the radiating mixed modes ($M1, M2$) and the transverse modes ($T1, T2$) in the spectral region of the isolated doubly-degenerate exciton state of a uniaxial crystal for a fixed direction of emission into vacuum at an angle φ . The inset at left shows the geometry used to measure the emission due to the mixed modes.

tal boundary. These waves do not cause energy transfer within the medium for $\Gamma = 0$, and therefore give no direct contribution to the external emission. However, for $\Gamma \neq 0$ the surface radiating modes are partially included in the energy transfer within the medium,⁶ and consequently we should expect a well-defined contribution to the crystal luminescence from these modes.

The dispersion intervals for the nonuniform surface-radiating waves are actually shown in Fig. 1: they lie in the region to the left of the point where $T2$ and $M2$ intersect. To the right of this point, for $\Gamma = 0$ the dispersion curves represent well-defined quantum (polariton) states of the crystal. This same point of intersection corresponds to a zero value of the normal components of the wave vectors of the modes at the sample surface.

In analyzing the process of light emission when the dissipative attenuation Γ is taken into account, we should keep in mind that near the frequency ω_L the value of $|\text{Im } \mathbf{K}_\beta|$ becomes comparable to $|\text{Re } \mathbf{K}_\beta|$ for the PUB, and that the corresponding modes are, generally speaking, nonuniform.¹³ Furthermore, in this particular region of the spectrum, nearby values acquire real parts equal to the wave vectors of the mixed modes $M1$ and $M2$, especially when the direction of propagation is close to $\mathbf{K} \perp \mathbf{C}$. This implies that the criteria (1), (2) for applicability of the kinetic equation are clearly violated for polaritons on the $T2$, $M2$, and $M1$ branches near the frequency ω_L .

The inset to Fig. 1 shows the experimental geometry used to measure the radiation of the mixed modes $M1$ and $M2$. In this experimental geometry it is possible to change the longitudinal-transverse splitting $\tilde{\omega}_{LT}$ [see (6), (7)] by choosing φ , i.e., the exit angle of the radiation ($\sin \varphi = K_x/k_0$). In this connection, the form of the mixed-mode dispersion relation given by Eq. (6) turns out to be very convenient, since the dispersion relations for the transverse modes (5) and mixed modes (6) become formally equivalent: Eq. (6) differs from Eq. (5) only in containing a different "resonant" frequency (ω_L in place of ω_0) and a different "longitudinal-transverse" splitting ($\tilde{\omega}_{LT}$ in place of ω_{LT}).

At this point we should add that under these experimental conditions the emission spectrum is measured for fixed values of φ (or $\tilde{\omega}_{LT}$), i.e., for a fixed projection K_x of the wave vector (i.e., the same for all the radiating modes). This implies that for the radiating modes the angles θ_β between \mathbf{K}_β and \mathbf{C} inside the crystal are variables (i.e., they depend on the frequency ω) and the dispersion relation (6) determines which state emits light in the external direction given by the angle φ (the corresponding solutions to this equation are shown schematically in Fig. 1 by the curves $M1$ and $M2$). For nonzero values of Γ , the angles θ_β become complex, and when Γ is large enough, the concept of an intensity within the radiating medium loses its meaning.

Corresponding to the conditions of the experiment, we will assume that excitation of low-temperature PL comes about by steady-state illumination of the crystal with light whose wavelength lies in the spectral region of intrinsic absorption, so that this absorption results in the generation of free electrons and holes. As these carriers thermalize, they are bound into excitons which in turn undergo multiple scattering by phonons, impurities, and crystal defects, thereby relaxing in energy and momentum into the resonance region

where a certain steady-state polariton distribution function is established.

Usually the inequality $\varepsilon_b \omega_\mu \ll \omega_{LT}$, where $\omega_\mu = \hbar k_0^2 / 2\mu$ ($\mu = M_1, M_{\parallel}$), is satisfied for dipole-active excitons. Therefore the densities of states

$$\rho_\beta(\omega) = \sum_{\mathbf{k}} \delta(\omega - \omega_{\mathbf{k}}^{(\beta)})$$

for polaritons of branches $\beta' = T1, M1$ and $\beta'' = T2, M2$ differ strongly (for $\Gamma \rightarrow 0$): $\rho_{\beta''} \ll \rho_{\beta'}$. For the $M1$ branch the density of radiating K -states near the frequency ω_L is considerably smaller than the densities of all the other (nonradiating) states of type $M1$ and the densities of states for the $T1$ branches. Consequently, in the neighborhood of the frequency ω_L we can neglect completely the scattering of waves within the branches $T2, M2$, while within $M1$ we can partially neglect it (in any case, for the radiating states). For this reason, we can ignore the generation of $T2, M2$, and $M1$ waves (with small values of $|\mathbf{K}|$) caused by LO phonon scattering from higher-lying exciton states, and also any possible scattering of the PLB induced by multiple internal specular reflection from the surface.⁵

Thus, we can assume that the distribution function f of polaritons is essentially determined by the relaxation of these polaritons through transverse $T1$ ($f_{T1\mathbf{K}}$) and nonradiating mixed ($f_{M1\mathbf{K}}$) mode states. Finding the precise form of these functions goes beyond the framework of the present article. It is sufficient for our purposes to limit ourselves to the simplest factorized form:⁴

$$f_{\beta\mathbf{K}}(\omega, z) = f_{\beta\mathbf{K}}(\omega) \exp(-z/L), \quad (8)$$

which includes a certain smooth function of ω near ω_L (where L is the effective spatial decay length of the polariton distribution, determined by processes of multiple scattering by free carriers and excitons). The fact that $f_{\beta\mathbf{K}}(\omega, z)$ depends only on z is a consequence of the uniformity of the problem along the plane of the surface.

In the experimental geometry of interest to us, only the mixed modes $M1$ and $M2$ give a contribution to the spectral intensity $I = I_p^{(0)}(\omega, \Omega)$ of p -polarized radiation propagating outside the crystal in the direction of the unit vector $\Omega = \mathbf{k}_0/k_0$ ($k_{0x}/k_0 = \sin \varphi$, see the inset of Fig. 1). For the reasons presented above, we can assume that radiating states of the $M1$ and $M2$ branches are populated because of single scattering of $T1$ polaritons and nonradiating $M1$ polaritons according to the distribution functions specified in (8). By introducing these distribution functions, we limit ourselves to those values of the attenuation parameter for which the conditions of applicability of the kinetic equation are fulfilled for the $T1$ states and nonradiating $M1$ states.

2. Theoretical calculation

In order to calculate the intensity of emission $I_p^{(0)}(\omega, \Omega)$ we make use of the Keldysh diagram technique, which is generalized in order to discuss exciton kinetics (see Ref. 13, where a case in which condition (1) is violated is discussed for the first time in treating the kinetics of transverse polariton modes of the upper dispersion branch of the crystal ZnP_2). The necessary Green's function has the matrix form

$$\hat{G} = \begin{pmatrix} G^{--} & G^{-+} \\ G^{+-} & G^{++} \end{pmatrix},$$

where

$$G^{\alpha\alpha'}(nt, n't') = -i \text{Sp} [\rho_0 \hat{T}_c \hat{a}_n(t_\alpha) \hat{a}_{n'+}^\dagger(t_{\alpha'}) \hat{s}_c],$$

ρ_0 is the density matrix for noninteracting excitons, \hat{T}_c is an operator which orders the lines of the diagram, \hat{a}_n^+ and \hat{a}_n are creation and annihilation operators

$$\hat{s}_c = \exp\left(-\frac{i}{\hbar} \int_c \hat{V}(\tau) d\tau\right),$$

and $\hat{V}(\tau)$ is the interaction operator in the Heisenberg representation.

Let us discuss the Fourier components of the Green's function $G_{\beta}^{-+}(\mathbf{K}, \mathbf{K}', \omega)$ for the mixed modes $\beta = M1, M2$ for a specified $T1$ and $M1$ polariton distribution function, taking into account the distinctive features of the scattering processes noted in the preceding paragraph. The diagrams for the function $G_{\beta}^{-+}(\mathbf{K}, \mathbf{K}', \omega)$ are represented in Fig. 2, where the heavy solid lines denote exciton Green's functions renormalized by photon-exciton, exciton-lattice, and other interactions:

$$G_{M\mathbf{K}\omega}^{--} = [\omega - \omega_{\mathbf{K}}^{(M)} + i\Gamma(\omega, \mathbf{K})/2]^{-1},$$

$$G_{M\mathbf{K}\omega}^{+\pm} = -(G_{M\mathbf{K}\omega}^{--})^*, \quad (9)$$

$$G_{\beta\mathbf{K}}^{-+}(\omega, z) = 2\pi f_{\beta\mathbf{K}}(\omega, z) \delta(\omega - \omega_{\mathbf{K}}^{(\beta)}), \quad \beta = T1, M1.$$

Here $\omega_{\mathbf{K}}^{(M)}$ is given by Eq. (7), while $\omega_{\mathbf{K}}^{(T1)}$ and $\omega_{\mathbf{K}}^{(M1)}$ are given by Eqs. (4) and (7) respectively; $\Gamma(\omega, \mathbf{K})$ is the exciton attenuation due to scattering and capture processes. The Green's function $G_{M\mathbf{K}\omega}^{--}$ can be represented in the form of a sum of two pole terms

$$G_{M\mathbf{K}\omega}^{--} = \sum_{j=1,2} G_{Mj\mathbf{K}\omega}^{--}, \quad (10)$$

$$G_{Mj\mathbf{K}\omega}^{--} = (-1)^j \frac{2M_{\parallel}}{\hbar} \frac{\mathbf{K}_{Mj}^2 - \varepsilon_b k_0^2}{\mathbf{K}_{M1}^2 - \mathbf{K}_{M2}^2} \frac{1}{\mathbf{K}^2 - \mathbf{K}_{Mj}^2}$$

where \mathbf{K}_{Mj} is the solution to the dispersion relation (6).

In calculating $I_p^{(0)}(\omega, \Omega)$, the Green's function $G_{\beta\mathbf{K}}^{--}$ and $G_{Mj\mathbf{K}\omega}^{+\pm}$ correspond to the upper and lower exciton lines shown in Fig. 2. Note that for $\beta = T1, M1$ we need not include diagrams for $G_{\beta\mathbf{K}}^{--}(\omega, z)$ and $G_{\beta\mathbf{K}}^{+\pm}(\omega, z)$ with external lines corresponding to scattering via the states ($T1, \mathbf{K}$) and the nonradiating states ($M1, \mathbf{K}$), since the distribu-

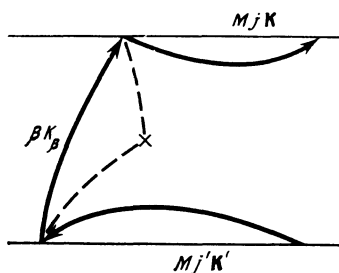


FIG. 2. Diagram for the Green's function $G_{Mj\mathbf{K}\omega}^{+\pm}$; $j, j' = 1, 2$; $\beta = T1$.

tion functions $f_{T1\mathbf{K}}(\omega, z)$ and $f_{M1\mathbf{K}}(\omega, z)$ are considered to be prespecified.

The spectral intensity of the luminescence $I_p^{(0)}(\omega, \Omega)$ is determined by the amplitudes of the transmission coefficients $t_{0\beta}^{(p)}$ from the crystal into the external medium, and by the amplitudes of the electric field intensity vectors $\mathbf{E}_{\beta}(\mathbf{K}_{\perp}, \omega; z = z_0)$ of the mixed modes with frequency ω and wave vector component $\mathbf{K}_{\perp} = k_0 \Omega_{\perp}$, with $\Omega_{\perp} = (\Omega_x^2 + \Omega_y^2)^{1/2}$, at the boundary of the crystal $z = z_0$:

$$I_p^{(0)}(\omega, \Omega) = \frac{1}{8\pi} \frac{k_0^2}{(2\pi)^3} \left\langle \left| \sum_{\beta=M1, M2} t_{0\beta}^{(p)} \mathbf{E}_{\beta}(\mathbf{K}_{\perp}, \omega; z=z_0) \right|^2 \right\rangle, \quad (11)$$

The sign $\langle \dots \rangle$ denotes averaging with respect to the ensemble of scattering particles and with respect to the direction of the polarization and propagation of the scattered wave.

By adding the supplementary boundary conditions (SBC) of Pekar¹⁵ to the Maxwell boundary conditions, and by taking into account the presence of a nonexcitonic "dead" layer of thickness l at the surface of the crystal,¹⁶ we obtain for the quantity $t_{0\beta}^{(p)}$ the expression

$$t_{0\beta}^{(p)} = \frac{n_{\beta z} n_{0x} / n_{0z}}{[n_{\beta z}^2 n_{0x}^2 + (n_{\beta z}^2 - \varepsilon_b)^2]^{1/2}} \frac{2\bar{n}_p}{(1 + \bar{n}_p) \cos \delta - i(\chi + \bar{n}_p / \chi) \sin \delta}, \quad (12)$$

where

$$\bar{n}_p = \frac{n_{0z} \varepsilon_b (n_{M1z} + n_{M2z})}{n_0^2 (\varepsilon_b - n_{0x}^2 + n_{M1z} n_{M2z})},$$

$$\chi = \frac{n_{0z} \varepsilon_b}{n_0^2 (\varepsilon_b - n_{0x}^2)^{1/2}},$$

$$n_{0z} = n_0 \cos \varphi, \quad n_{0x} = n_0 \sin \varphi, \quad n_{\beta z} = (n_{\beta}^2 - n_{0x}^2)^{1/2},$$

$$\delta = \varepsilon_b k_0 l / (\varepsilon_b - n_{0x}^2)^{1/2},$$

n_0 and $n_{\beta} = (\mathbf{K}_{\beta}^2)^{1/2} / k_0$ are the indices of refraction of the surrounding medium and the crystal for the modes $M1$ and $M2$.

In order to calculate the quantities $\mathbf{E}_{\beta}(\mathbf{K}_{\perp}, \omega; z = 1)$ it is convenient to decompose $\mathbf{E}_{\beta}(\mathbf{K}, \omega; z)$ into its longitudinal and transverse components $\mathbf{E}_{\beta}^{\text{long}} = (\mathbf{E}_{\beta} \mathbf{K}_{\beta}) \mathbf{K}_{\beta} / \mathbf{K}_{\beta}^2$ and $\mathbf{E}_{\beta}^{\text{tr}} = \mathbf{E}_{\beta} - \mathbf{E}_{\beta}^{\text{long}}$ with respect to the wave vector \mathbf{K}_{β} ; for the mixed modes, these components are related by the expression

$$\mathbf{E}_{\beta}^{\text{long}} = -\frac{K_{\beta i} \varepsilon_{ij}(\omega, \mathbf{K}_{\beta}) E_{\beta j}^{\text{tr}}}{k_0 n_{\beta} \varepsilon_{\text{long}}(\omega, \mathbf{K}_{\beta})}, \quad (13)$$

where

$$\varepsilon_{\text{long}}(\omega, \mathbf{K}_{\beta}) = K_{\beta i} K_{\beta j} \varepsilon_{ij}(\omega, \mathbf{K}_{\beta}) / \mathbf{K}_{\beta}^2.$$

From the Maxwell equations, we establish the following relation between the exciton polarization \mathbf{P}_{β} and the component $\mathbf{E}_{\beta}^{\text{tr}}$ of the intensity:

$$4\pi \mathbf{P}_{\beta} n_{0x} / n_{\beta} = (n_{\beta}^2 - \varepsilon_b) \mathbf{E}_{\beta}^{\text{tr}},$$

on the basis of this expression, it is easy to find a relation connecting \mathbf{P}_{β} and $\mathbf{E}_{\beta}^{\text{long}}$ by using (14).

Using the rules of the diagram technique, we obtain

$$\begin{aligned} & \langle \mathbf{E}_\beta(K_\perp, \omega; z) \mathbf{E}_{\beta'}^*(K_\perp, \omega; z) \rangle \\ &= A \sum_{\beta'=T1, M1} \sum_{\mathbf{K}_{\beta'}} \sum_j \mathcal{F}_{\beta K_\perp \omega}(\mathbf{K}_{\beta'}; z, z_j) \\ & \quad \times \mathcal{F}_{\beta' K_\perp \omega}^*(\mathbf{K}_{\beta'}; z, z_j) G_{\beta' \mathbf{K}_{\beta'}}^+(\omega, z), \end{aligned} \quad (14)$$

where

$$\beta, \beta' = M1, M2;$$

$$\begin{aligned} & \mathcal{F}_{\beta K_\perp \omega}(\mathbf{K}_{\beta'}; z, z_j) \\ &= \sum_{k_z} G_{\beta K \omega}^- \left[\frac{n_{0x}^2/n_\beta^2}{(n_\beta^2 - \varepsilon_\beta)^2} + \frac{n_{\beta z}^2/n_\beta^2}{\varepsilon_\beta^2} \right]^{1/2} \exp[iK_z(z - z_j)] \\ & \quad \times V(\mathbf{K}_{\beta'} - \mathbf{K})(\mathbf{e}_{\beta'}(\mathbf{K}_{\beta'}) \mathbf{e}_\beta(\mathbf{K})), \end{aligned} \quad (15)$$

A is a constant, z_j is the coordinate of the j th scattering center, $V(\mathbf{q})$ is the Fourier transform of the perturbing potential ($\mathbf{q} = \mathbf{k}_\beta' - \mathbf{k}$), and $\mathbf{e}_{\beta'}$ and \mathbf{e}_β are unit polarization vectors for the waves $\beta' = T1, M1$ and $\beta = M1, M2$. In carrying out the summation Σ' with respect to \mathbf{K}_{M1} , it is necessary to exclude the radiating states of type $M1$. It is useful to note that the magnitudes $|\mathbf{K}|$ of the wave vectors of the radiating states are considerably smaller than the magnitudes $|\mathbf{K}'|$ of the wave vectors of the scattered waves, and therefore we can replace $V(\mathbf{K}' - \mathbf{K})$ in (14) by $V(\mathbf{K}')$.

Substituting (9), (10) into (14), (15), we finally obtain

$$I_p^{(0)}(\omega, \Omega) = \sum_{\beta=M1, M2} I_{p, \beta}^{(0)}(\omega, \Omega) + I_{p, M12}^{(0)}(\omega, \Omega), \quad (16)$$

$$I_{p, \beta}^{(0)}(\omega, \Omega) = F(\omega, \Omega) |\mathcal{F}_\beta(\omega, \Omega)|^2 / (2k_0 \text{Im} n_{\beta z} + L^{-1}), \quad (16a)$$

$$I_{p, M12}^{(0)}(\omega, \Omega) = -F(\omega, \Omega) \cdot 2 \text{Re} \left[\frac{\mathcal{F}_{M1}(\omega, \Omega) \mathcal{F}_{M2}^*(\omega, \Omega)}{-ik_0(n_{M1z} - n_{M2z}) + L^{-1}} \right], \quad (16b)$$

where

$$F(\omega, \Omega) = \frac{1}{(2\pi)^3} \frac{2M \parallel^2 c \varepsilon_b \omega_{LT} \cos \varphi}{\hbar |n_{M1}^2 - n_{M2}^2|^2} \sum_{\beta'=T1, M1} \sum_{\mathbf{K}_{\beta'}} \frac{f_{\beta' \mathbf{K}_{\beta'}}(\omega)}{\tau_{M\beta' \mathbf{K}_{\beta'}}}, \quad (17)$$

$$\mathcal{F}_\beta(\omega, \Omega) = \frac{t_{0\beta}^{(p)}(\omega, \Omega)}{n_{\beta z}} \left[\frac{(n_\beta^2 - \varepsilon_\beta)^2}{\varepsilon_\beta^2} \frac{n_{\beta z}^2}{n_\beta^2} + \frac{n_{0x}^2}{n_\beta^2} \right]^{1/2}, \quad (17a)$$

while the quantity

$$\frac{1}{\tau_{M\beta' \mathbf{K}_{\beta'}}} = \frac{2\pi}{\hbar^2} N \cdot \frac{1}{2} |V(\mathbf{K}_{\beta'})|^2 \delta(\omega - \omega_{\mathbf{K}_{\beta'}}^{(\beta')}) \quad (18)$$

is the inverse decay time for the states ($M1, \mathbf{K}$) or ($M2, \mathbf{K}$) into the polariton states ($\beta', \mathbf{K}_{\beta'}$) per unit solid angle in the neighborhood of the direction $\mathbf{K}_{\beta'}$, and N is the concentration of scattering centers. In this case, (16b) describes the interference-produced contribution of the mixed modes $M1$ and $M2$ to the intensity of external radiation $I_p^{(0)}$, connected with scattering of polaritons of branches $M1, T1$ into coherently radiating states $M1$ and $M2$ by the same center.

Thus, Eq. (16) allows us to calculate the luminescence spectrum of the mixed modes — including the nonuniform ones — in the presence of attenuation, where the approximation of the kinetic equation is violated. By using this ap-

proach, we succeed in surmounting the principal difficulty connected with using the concept of emission intensity in an absorbing medium by operating only with the field amplitudes.

III. EXPERIMENT

In order to investigate experimentally the distinctive features of the mixed-mode PL, we used crystals of CdS grown by the gas-transport method.¹¹ The crystalline samples consisted of films of thickness about 0.1 mm, with mirror-smooth natural growth facets with the optical (hexagonal) C axis oriented in the plane of the radiating facets. We carried out a preliminary spectroscopic selection among the samples, allowing us to choose crystals with high structural perfection and optical quality. Special attention was paid to the choice of crystals in which the low-temperature spectra of spectral reflection had the standard form¹⁷⁻¹⁹ which is most often encountered, and which is accurately described by means of the “dead” layer (DL) model employing the additional Pekar boundary conditions.¹⁵

The samples were immediately immersed in pumped-out liquid helium at a temperature of 2 K. The construction of the crystal holder we used allowed independent rotation of the sample in the optical cryostat around both the vertical and the horizontal axes. The angle of rotation about the vertical-axis rod was measured with an error of less than $\pm 0.1^\circ$ by measuring the deflection of a laser beam reflected from a mirror rigidly clamped to this axis. Corresponding to the experimental geometry shown in the inset to Fig. 1, the C -axis of the crystal was oriented horizontally, i.e., perpendicular to the rod axis (i.e., the y -axis).

The spectrum was recorded using an apparatus assembled around a DFS-24 spectrometer operating in the photon-counting regime with a minimum spectral slit width of 0.05 meV under conditions of maximum possible spectral resolution. The light used to excite the PL came from an Ar^+ laser focused on the crystal surface within a spot (strip) with dimensions $\sim 0.4 \times 4 \text{ mm}^2$; the wavelength of the light was $\lambda \simeq 476.5 \text{ nm}$, while the optical beam power was $\sim 7 \text{ mW}$. This relatively weak illumination did not lead to any appreciable change in the spectrum of specularly reflected light.

The angular resolution $\Delta\varphi$ (with respect to the output radiation angle φ , specified by rotating the rod around the vertical axis) was limited by the minimum working aperture of the objective, which was located in front of the input slit of the spectrometer; $\Delta\varphi \simeq 1^\circ$ for $\varphi \lesssim 15^\circ$ to 20° , while $\Delta\varphi \simeq 6^\circ$ for $\varphi > 20^\circ$. This increase in $\Delta\varphi$ at large angles leads to a subsidiary loss of angular resolution; however, this loss is balanced by the possibility of reliably reproducing the fine structure of the emission spectrum under the most favorable signal-to-noise conditions.

The experimental geometry corresponding to the theoretical situation described in Chapter II is realized in the spectral region of the lowest exciton state $A_{n=1}$ of cadmium sulfide for light polarized so that $\mathbf{E} \perp [\mathbf{C}\mathbf{K}]$. The emission spectra of CdS crystals at $T = 20 \text{ K}$ was already studied in Ref. 12, in which there was a discussion of the variation of the intensity and shape of the luminescence line A_L of a mixed polariton. However, in light of the results of Chapter II, an analysis of the spectra carried out by using the arguments of purely polariton kinetics (i.e., without taking into account broadening of the polariton state) is unjustified (the

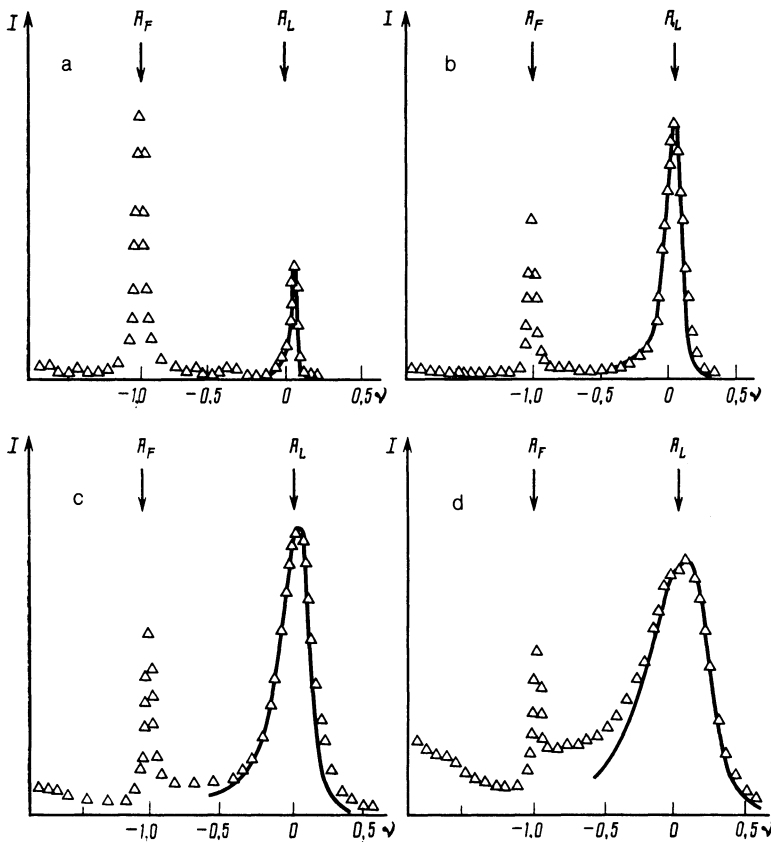


FIG. 3. Luminescence spectra of CdS crystals (the exciton state $A_{n=1}$, $T = 2$ K) in the mixed mode emission geometry (see inset to Fig. 1) for the output emission angles $\varphi = 2.5^\circ$ (a), 15° (b), 30° (c), and 67.5° (d). The points are experiment, the smooth curves are theory.

more so since in Ref. 12 these arguments were applied to a relatively high-temperature experimental situation). In our case, the choice of $T = 2$ K has the considerable merit that only at low temperatures is the exciton attenuation Γ small enough¹⁶ for the criteria for applicability of the kinetic equation to be fulfilled for those polariton branches which provide the initial states for scattering into the radiating mixed mode states.

Typical PL spectra of the mixed modes measured at $T = 2$ K for various output angles φ are shown in Fig. 3: $\varphi = 2.5^\circ$ (a), 15° (b), 30° (c) and 67.5° (d). Along the abscissa we plot the relative frequency $\nu = (\omega - \omega_L)/\omega_{LT}$. The line A_L is localized near the value $\nu = 0$; its intensity rapidly increases with increasing φ . Orientation of the C axis relative to the direction in which the emission was measured at which the line A_L completely disappears, allows us to establish an absolute reference point $\varphi = 0^\circ$ for the output angle.

As the angle φ increases, the width of the line A_L also increases along with its maximum intensity I_{AL} . In this case, starting with certain angles $\varphi \gtrsim 30^\circ$, we have observed a fine doublet structure in the spectrum of A_L (Fig. 3d). The shape of this structure is modified at large angles, and disappears for sufficiently large values $\varphi \gtrsim 75^\circ$. The way the observed fine structure develops on the line A_L can be seen in Fig. 5 plotted on a rough scale. In this figure, the experimental data are presented for five output emission angles: $\varphi = 30^\circ$ (1), 45° (2), 60° (3), 75° (4), and 80° (5).

It is convenient to measure the function $I_{AL}(\varphi)$ using I_{AF} , the intensity of the emission line A_F of the orthoexciton state of symmetry Γ_6 localized near the frequency $\nu = -1$

(see Fig. 3), as a reference intensity. The narrow line A_F is connected with a dipole-forbidden state of the exciton; its intensity $I_{AF}(\varphi)$ is primarily determined by the φ -dependence of the Fresnel transmission coefficient for the polarization $E \perp [CK]$ at the frequency A_F . In the interval $0 \leq \varphi < 30^\circ$ this dependence is practically undetectable. By normalizing I_{AL} with the intensity I_{AF} , we can greatly increase the accuracy of our measurement of the function $I_{AL}(\varphi)$.

This dependence is illustrated in Fig. 6 by plotting the experimental points in the form of the ratio $I_{AL}(\varphi)/I_{AF}$ (see below). The behavior of the half-width of the emission line A_L as φ varies is shown in Fig. 9 (see below): the experimental points are plotted after subtracting the instrumental spectral width ~ 0.05 meV.

IV. COMPARISON OF THE EXPERIMENTAL AND THEORETICAL DATA; DISCUSSION OF RESULTS

The calculations of the PL spectra of the mixed modes were carried out using Eq. (16) from the theory given in Chapter II, for the following parameter values of the exciton resonance $A_{n=1}$ of the CdS crystal: $\hbar\omega_0 = 2552.4$ meV, $\hbar\omega_{LT} = 2$ meV, $\hbar\Gamma = 0.075$ meV, $\epsilon_b = 9.3$, $M_\perp = 0.9 m_0$ (m_0 is the mass of the free electron), $M_\parallel = 2.85 m_0$, $l = 70$ Å, and $L = 0.8 \mu\text{m}$. These values of the parameters are in good agreement with data on Brillouin resonant scattering²⁰ and on excitonic reflection of light,¹⁶⁻¹⁹ including the spectra of CdS crystals measured in this paper.

In the narrow spectral region occupied by the line A_L we can neglect the smoothly-varying frequency dependence of the distribution functions f_{T1} and f_{M1} for the polaritons

which undergo the scattering, and also the lifetimes $\tau_{\beta\beta'}^{-1}$ ($\sum_{\mathbf{K}\beta} \tau_{\beta\beta'}^{-1} = \Gamma$) with respect to emission from the radiating state (β' , \mathbf{K}). For this particular region of the spectrum the value of Γ is essentially determined by the exciton reflection spectra at low temperatures.¹⁶

The calculated PL traces are compared with experimental data in Fig. 3 (solid traces are theory). It is clear from Fig. 3 that the experimental and theoretical spectra are in good agreement, given the assumptions we have made and the parameter values we have chosen. In this case it is important to emphasize that the only parameter whose variation turns out to affect the curves is the effective spatial decay length of the distribution L . The remaining parameters are fixed by the other experimental data.

On comparing the experimental and theoretical results more carefully, we note certain discrepancies in the short-wavelength region of the spectrum for small angles ($\varphi < 30^\circ$) and in the long-wavelength region for large angles ($\varphi > 30^\circ$). These discrepancies apparently can be avoided if we also include in the theory inelastic scattering channels into radiating states with relatively large values of $|\mathbf{K}|$ and the frequency dependences of the distribution functions $f_{T1}(\omega)$ and $f_{M1}(\omega)$. Furthermore, the observed additional radiation in the spectral interval between the lines A_L and A_F (especially at large angles φ) can indicate a certain repopulation of the radiating states $M1$ due to scattering of excitons from the parabolic band Γ^6 (by a scattering potential of ap-

propriate symmetry). In connection with this, it is also noteworthy that the intensity of the emission on the long-wavelength side of the line A_F , whose position practically coincides with the bottom of the exciton Γ_6 band, falls off abruptly.

The line A_L is not seen in the output radiation for the direction normal to the face of the crystal ($\varphi = 0^\circ$). In this case, the mixed modes are transformed into a pure longitudinal exciton mode and a pure transverse photon mode. The longitudinal exciton undergoes total internal reflection in the direction $\varphi = 0^\circ$, which the probability of scattering into a transverse photon state ($\mathbf{E} \parallel \mathbf{C}$, $\mathbf{K} \perp \mathbf{C}$) is negligibly small. Therefore, there is no $\mathbf{E} \parallel \mathbf{C}$ radiation from the crystal in this direction near the frequency ω_L . As the angle φ increases, the intensity of A_L emission increases, and at the same time its half-width grows; this correlates qualitatively with the increase in the "longitudinal-transverse" splitting $\tilde{\omega}_{LT} \propto \sin^2 \varphi$ (or, in other words, the oscillator strength of the transition).

The theoretical traces in Fig. 3 were plotted taking into account all the contributions to the luminescence from the mixed modes $M1$ and $M2$, as discussed Chapter II, 2. It is interesting to analyze in more detail the mechanisms which give rise to these traces. To do this, we show in Fig. 4 the spectral functions for the partial intensities $I_\beta(\omega, \varphi) = I_{p,\beta}^{(0)}(\omega, \Omega)$ caused by contributions to the external radiation from the mixed modes ($\beta = M1, M2$, traces 1 and 2),

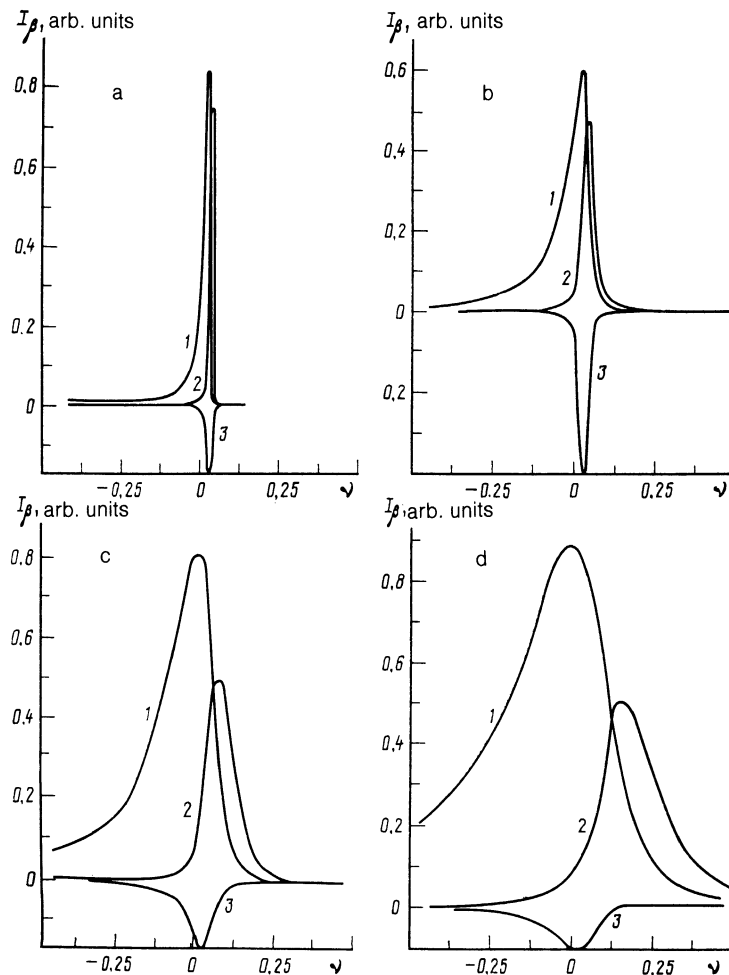


FIG. 4. Spectral dependence of the partial intensities I_{M1} , I_{M2} of the modes $M1$, $M2$ (curves 1, 2) and their interference contribution I_{M12} (curve 3), calculated for parameters of the exciton state $A_{n=1}$ in CdS at the output emission angles $\varphi = 2.5^\circ$ (a), 15° (b), 30° (c), and 67.5° (d).

taking into account their interference ($\beta = M12$, trace 3), for output angles $\varphi = 2.5^\circ$ (a), 15° (b), 30° (c) and 67.5° (d).

As the output angle φ increases, a considerable variation is observed in the intensities I_β and their spectral functions. In this case, special interest attaches to the interference contribution I_{M12} (traces 3), which enters in with opposite sign in the total intensity $I = I_p^{(0)}$ [see (16)]. It is clear from Fig. 4 that the negative intensity I_{M12} behaves nonmonotonically as φ increases; its magnitude reaches a maximum for a certain intermediate angle φ_c (it is found from numerical calculations that $\varphi_c \approx 9^\circ$).

In the interval $5^\circ < \varphi < 20^\circ$, the contribution I_{M12} to I is comparable to the partial intensities I_{M1} and I_{M2} , while for $\varphi = \varphi_c$ the value of I_{M12} near the frequency ω_L can even exceed I_{M1} and I_{M2} somewhat (of course, in this case we always have $|I_{M12}| < I_{M1} + I_{M2}$). As φ increases, we observe spectral broadening of all the components and a shift of the maximum of I_{M2} to shorter wavelengths. This behavior of the separate components leads to a complex change in the shape of the total spectrum $I = I_p^{(0)}$, which is especially noticeable at large output emission angles, where a doublet structure is observed in the maximum (see Fig. 3d).

Figure 5b demonstrates how the theoretical shape of the radiation maximum of A_L varies as the angle φ increases. It is clear that the theoretical traces in Fig. 5b reproduce the principal qualitative features of the experimental traces (Fig. 5a) quite well. The doublet structure appears within a certain range of output angles ($30^\circ < \varphi < 75^\circ$) both in theory and experiment. At large values of φ , the doublet structure disappears, while the maximum shifts to the short-wavelength side. Also noteworthy is a certain asymmetry in the shape of the spectral components I_β , which is most noticeable at small output angles. A comparison of Figs. 3a and 4a

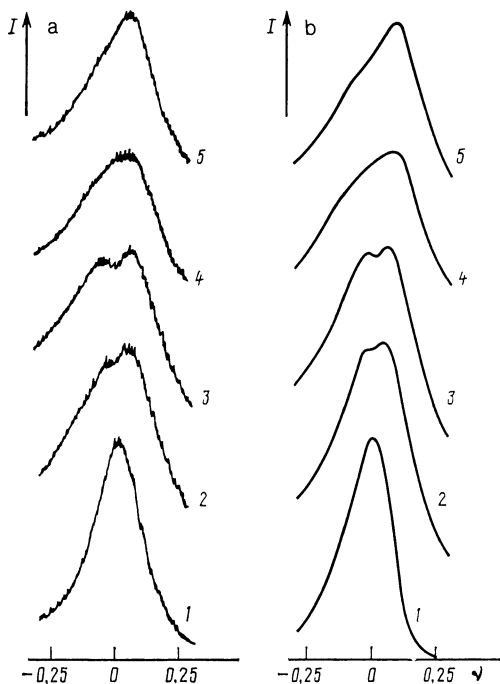


FIG. 5. Comparison of experimental (a) and theoretical (b) spectral line-shapes of the mixed-mode emission from CdS crystals (the exciton state $A_{n=1}$, $T = 2$ K) for the output angles $\varphi = 30^\circ$ (1), 45° (2), 60° (3), 75° (4) and 80° (5). The spectral width of the slit equals 0.05 meV.

shows that the observed narrow asymmetric profile of the emission A_L for $\varphi = 2.5^\circ$ is essentially due to asymmetry in the spectral contribution I_{M1} .

In order to correctly describe the experimental data given here, it is important to include all three terms in (16). In particular, the interference term I_{M12} affects the character of the variation in the spectral line shape of the total intensity as a function of the angle φ to a considerable degree, while the shift in the maximum of A_L noted above is connected with the short-wavelength shift with increasing φ in the maximum of the intensity I_{M2} .

As for the angular (i.e., φ) dependence of the maximum in the intensity $I_{\max} = I_{p,\max}^{(0)}$ (Fig. 6), it is very sensitive to the value of the spatial decay length of the polariton distribution L . The theoretical (solid) traces in Fig. 6 clearly illustrate this fact. The best agreement between theory and experiment is attained for $L = 0.8 \mu\text{m}$. It is clear from Fig. 6 that as φ increases the theoretical value $I_{\max}(\varphi)$ for a given L goes to a universal limiting value. In comparing the calculated traces with the experimental ones, this universal value is chosen to equal the measured ratio I_{AL}/I_{AF} in the region of large values of φ .

The value of L which corresponds to the experimental trace 4 in Fig. 6 is a characteristic of each specific CdS crystal sample. The measurements we have carried out on other samples show that the traces $I_{AL}(\varphi)/I_{AF}$ (and consequently the value of L as well) are generally different for different samples.

The angular dependence of the maximum of the emission intensity I_A is most strongly affected by interference between the radiating modes $M1$ and $M2$. Neglect of this interference leads to a fundamental qualitative change in the dependence $I_{\max}(\varphi)$, as is demonstrated by the inset in Fig. 6: curves 4 and 4' were plotted for $L = 0.8 \mu\text{m}$, neglecting and including the interference term I_{M12} , respectively. Note that curve 4' has a sharply-defined maximum, correspond-

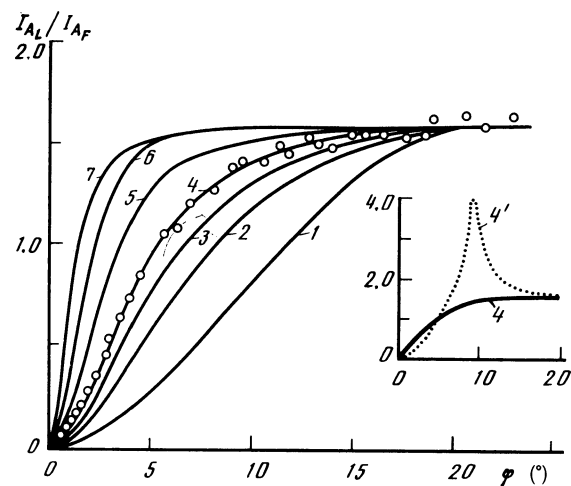


FIG. 6. Dependence on output angle φ of the ratio of the maximum spectral intensities of the emission lines A_L and A_F in crystals of CdS (the exciton state $A_{n=1}$, $T = 2$ K). The points are experiment, the theoretical traces 1–7 were calculated for various values of the effective spatial decay length of the polariton distribution $L = 0.1$ (1); 0.3 (2); 0.5 (3); 0.8 (4); 2.0 (5); 5.0 (6); and 10.0 (7) μm . In the inset we compare the theoretical functions $I_{AL}(\varphi)$, plotted including (curve 4) and neglecting (curve 4') the interference contribution I_{M12} for $L = 0.8 \mu\text{m}$.

ing to values of the output angle $\varphi = \varphi_c \approx 9^\circ$; this was mentioned earlier in connection with the discussion of Fig. 4.

It is clear from Fig. 6 that for increasing φ in the region $20^\circ > \varphi$ the theoretical traces $I_{\max}(\varphi)$ plotted for various values of L practically coincide with one another. This insensitivity of I_{\max} to the values of L for large values of the output angle is connected with the characteristic angular dependence of the imaginary parts of the indices of refraction $n_{\beta z}$ which appear in the expression (16a, 16b). If $\alpha = \min\{\alpha_1, \alpha_2\}$ is the smaller of the two values of absorption coefficient under discussion here, i.e., $\alpha_\beta = 2k_0 \text{Im } n_{\beta z}$ for the modes $\beta = M1, M2$, then it is clear from (16a, 16b) that the effect of L on the intensity of the radiation becomes insignificant when the condition $\alpha L \gg 1$ holds.

Using the formal similarity between the dispersion relations (5) and (6) for the transverse and mixed modes we have described above, we can easily generalize the results²¹ of theoretical investigations of isotropic absorption of light by excitons, taking into account spatial dispersion, to the case under discussion here of anisotropic absorption. In analogy with the approach of Ref. 21, we will discuss the behavior of the absorption coefficient α at the frequency $\omega = \omega_c$ for which a multiple root appears in the dispersion relation (6) for some value of $\Gamma = \Gamma_c$. Near this particular frequency, $\alpha(\omega)$ attains a maximum value for fixed values of Γ .

In our case, noting that the inequality

$$\left| 1 - \frac{M_\perp}{M_\parallel} \right| \sin^2 \varphi / \epsilon_b \ll 1$$

holds, we have

$$\begin{aligned} \omega_c &= \omega_L + \omega_\mu \epsilon_b, \\ \Gamma_c &= 4 \sin \varphi (\omega_\mu \omega_{LT})^{1/2}. \end{aligned}$$

The frequency ω_c , has a simple geometric meaning: it corresponds to the point where the dispersion curves for the transverse photons in the polarization $\mathbf{E} \parallel \mathbf{C}$ and the purely longitudinal excitons intersect (see Fig. 1).

In Fig. 7, the dependence of $\alpha_c = \alpha(\omega_c)$ on output angle φ is represented by the solid traces 1–4 for values of $\hbar\Gamma$ from 0.025 to 0.1 meV. These dependences are determined by the behavior of the quantities Γ_c as functions of φ . At some output angle $\varphi = \varphi_c$ determined by the condition $\Gamma_c = \Gamma$, a clearly-defined kink appears in the trace $\alpha_c(\varphi)$. This particular angle φ_c corresponds to the point of maximum interference of the radiating modes $M1$ and $M2$; for $\hbar\Gamma = 0.075$ meV (curve 3 of Fig. 7) we have $\varphi_c \approx 9^\circ$.

In the region to the left of the kink ($\varphi < \varphi_c$) we can reach the condition $\Gamma_c \ll \Gamma$, for which the effects of spatial dispersion on the mixed modes can be neglected, while the angular dependence of α_c takes the form

$$\alpha_c(\varphi) \approx 2k_0 \sin^2 \varphi \omega_{LT} / (\epsilon_b^{1/2} \Gamma).$$

For $\varphi \gtrsim \varphi_c$, the coefficient α_c depends weakly on φ , and is characterized by values close to the maximum value of the absorption coefficient when the light is polarized so that $\mathbf{E} \perp \mathbf{C}$ for the mixed modes (for $\hbar\Gamma = 0.075$ meV, $\alpha_c(\varphi \gtrsim \varphi_c) \approx 10^5 \text{ cm}^{-1}$).

It should be noted that the absorption coefficient α_c under discussion here is a meaningful measurable quantity for sufficiently thick crystalline films, i.e., films with thick-

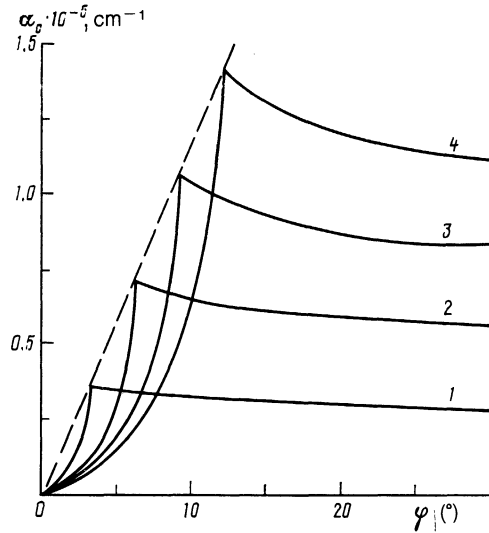


FIG. 7. Dependence on output angle φ of the absorption coefficient $\alpha_c = \alpha(\omega_c)$ of that mixed mode which has the smallest value of α_c at the frequency $\omega_c = \omega_L + \omega_\mu \epsilon_b$ for $\hbar\Gamma = 0.025$ (1); 0.05 (2); 0.075 (3); and 0.1 (4) meV.

ness $d \gg 2\alpha_c^{-1}$ (compare with Ref. 21). In the samples we used, the latter inequality does hold; however, in this case d is so large (~ 0.1 m) that for $\varphi \gtrsim \varphi_c$ the intensity of the light transmitted through the film at the frequency ω_c is practically unmeasurable. Therefore, under the conditions of our experiment it is impossible to study the behavior of the kink in the trace $\alpha_c(\varphi)$ at the angle φ_c by looking at the transmission spectrum of A_L .

As for the angular dependence of the maximum emission of A_L (see Fig. 6), we observed no singularity in this function (either in theory or in experiment) at the angle $\varphi = \varphi_c$. This is due to the fact that, in contrast to the transmission spectrum of light through a thin film, both modes $M1$ and $M2$ participate in the formation of the A_L emission spectrum near the frequency ω_c , resulting in a strong mutual interference contribution which smooths out the angular dependence of the total measured intensity.

In Fig. 8 we show a slice of the calculated isoenergetic surface $\omega = \omega_c$ for $A_{n=1}$ polariton emission in CdS ($\Gamma = 0$) through the xz measurement plane (\mathbf{C} is the crystal axis, $z = z_0$ is the "crystal-vacuum" boundary): a shows the overall shape, b the region of small values of $|\mathbf{K}|$. As we see, the isoenergetic surfaces $M1$ and $M2$ of the mixed modes pass smoothly into each other at $\theta = 90^\circ$ ($\varphi = 0^\circ$), having a circle in the yz plane as a curve of osculation. This osculation of the surfaces $M1$ and $M2$ occurs only for the frequency ω_c ; the osculation curve corresponds to states of purely longitudinal excitons ($\mathbf{E} \perp \mathbf{C}$) and transverse photons ($\mathbf{E} \parallel \mathbf{C}$).

The region of radiating states is included between the two horizontal dashed lines $x = k_0$ and $x = -k_0$ (i.e., the cross-section of a cylinder in \mathbf{K} -space). It is clear from Fig. 8b which states on the surface $M1$ and $M2$ contribute to the radiated light propagating at an output angle φ to the normal (with wave vector \mathbf{K}_0). For small angles φ , the radiating states $M1$ and $M2$ are positioned next to each other in \mathbf{K} space; this also ensures that the interference effect will be present for small values of Γ .

A comparison of the calculated and measured dependence of the half-width Δ of the emission line A_L on the angle

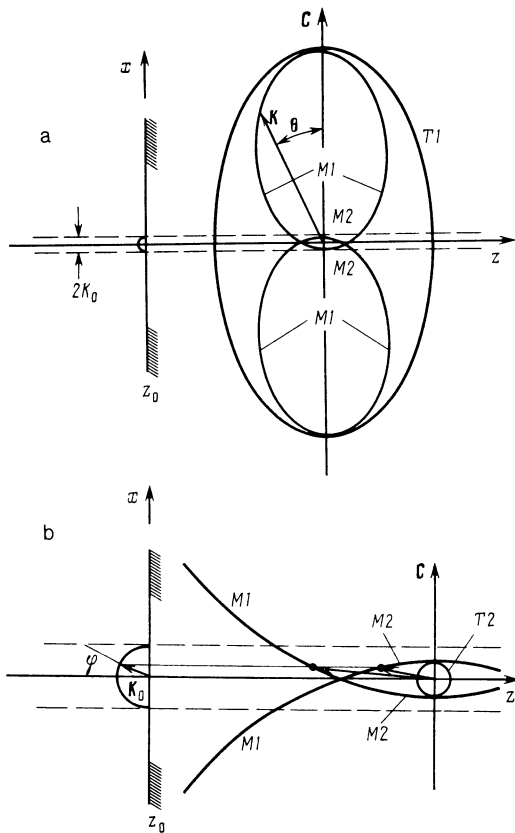


FIG. 8. Cross-section of the isoenergetic surface $\omega = \omega_c$ for $A_{n=1}$ polaritons in CdS ($\Gamma = 0$) when the emission is measured in the xz plane (see Fig. 1) (C is the crystal axis, $z = z_0$ is the crystal-vacuum interface): a is the general form, b is the region of small values of $|K|$. The states radiating into $M1$ and $M2$ (Fig. b) are specified by the output angle (i.e., the component K_{0x}).

φ is shown in Fig. 9. The theoretical trace (solid) is in good agreement with the experimental points. Nonmonotonic behavior in Δ is observed for increasing φ in the region of large values of φ ($\varphi \gtrsim 70^\circ$): the line A_L ceases to broaden and there is even a rather small narrowing for $\varphi > 80^\circ$. The function $\Delta(\varphi)$ qualitatively correlates with the character of the variation of the longitudinal-transverse splitting $\omega_{LT} \propto \sin^2 \varphi$, excluding the region where the narrowing occurs; in this region there is a decrease in the contribution of the partial intensity I_{M1} to the measured total intensity of the radiation.

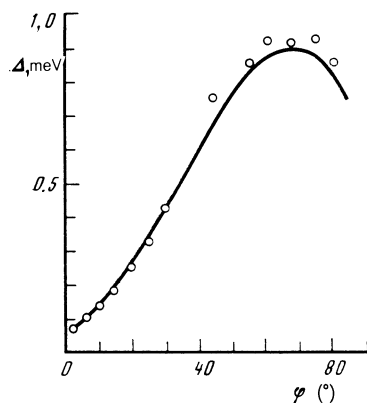


FIG. 9. Dependence on output emission angle φ of the half-width of the emission line A_L in CdS for $T = 2$ K: the points are from experiment, the solid curve is theory.

V. CONCLUSION

The theoretical and experimental investigation of the PL of mixed modes in an anisotropic crystal described in this paper shows that under conditions where the dissipative attenuation Γ of an exciton violates the criterion of applicability of the Boltzmann kinetic equation, the process of generation of the PL spectrum has a number of new and specific features. First of all, the reconstruction of the spectrum of normal modes for $\Gamma \neq 0$ leads to the inclusion in the energy transfer through the crystal boundary of surface-radiating modes (including the nonuniform ones), so that these modes make a direct contribution to the overall intensity of emission at frequencies $\omega \lesssim \omega_L$. Secondly, the presence of spatial dispersion gives rise to an interference interaction between the mixed modes, which is manifest in the excitation at the boundary of the crystal of an additional (interference-produced) energy current. This interference-produced contribution to the measured luminescence intensity is found to be comparable in absolute value to the individual contributions of the separate modes when the values of Γ and the angle φ of the output radiation from the crystal correspond to a multiple root of the dispersion relation for the radiating mixed modes.

The mechanism for generation of the PL discussed here includes the process of elastic scattering of polaritons from quantum states with well-defined wave vectors, i.e., with relatively large values of $|K|$, into radiating states of the mixed modes. The distribution function of the polaritons being scattered is characterized by an effective spatial decay length L for the exponential attenuation of the spatial distribution. The value of L is uniquely determined by the dependence of the maximum in the luminescence spectral intensity on the output angle φ . For this case, L is the only significant variable parameter of the theory, since the values of all the other parameters are specified by other experimental data.

The good quantitative agreement between the experimental data presented here on low-temperature exciton luminescence in CdS crystals and the results of theoretical calculations confirms the validity of the theoretical approach developed in this paper. This approach can be successfully used to describe the process of generation of the PL spectra in all cases where the light emission comes about through excitation of states with short lifetimes because of scattering (not necessarily only elastic scattering) into these states of polaritons (excitons) from well-defined initial quantum states.

In conclusion, we thank E. L. Ivchenko for his assistance in choosing the method of theoretical analysis, and for fruitful discussions regarding the questions treated in this article.

¹We are grateful to Sv. A. Pendyur and O. N. Talenskii for supplying the samples.

²V. M. Agranovich and M. D. Galanin, *Electronic Excitation Energy Transfer in Condensed Matter*. Elsevier, New York (1982) Ch. IV.

³M. S. Brodin, E. N. Myasnikov, and S. V. Marisova, *Polaritons in Crystal Optics*. Nauk. Dumka, Kiev, 1984.

⁴A. B. Pevtsov, A. V. Sel'kin, N. N. Syrby, and A. G. Umanets, *Zh. Eksp. Teor. Fiz.* **89**, 1155 (1985) [*Sov. Phys. JETP* **62**, 665 (1985)].

⁵E. L. Ivchenko, G. E. Pikus, and N. Kh. Yuldashev, *Zh. Eksp. Teor. Fiz.*

- 80, 1228 (1981) [Sov. Phys. JETP **53**, 629 (1981)].
- ⁶A. V. Sel'kin Fiz. Tverd. Tela (Leningrad) **19**, 2433 (1977) [Sov. Phys. Solid State **19**, 1424 (1977)].
- ⁷J. J. Hopfield and D. G. Thomas, Phys. Chem. Solids **12**, 276 (1960).
- ⁸S. A. Permogorov, A. B. Sel'kin and V. V. Travnikov, Fiz. Tverd. Tela (Leningrad) **15**, 1822 (1973) [Sov. Phys. Solid State **15**, 1215 (1973)].
- ⁹M. V. Lebedev, V. G. Lysenko, and V. V. Timofeev, Zh. Eksp. Teor. Fiz. **86**, 2193 (1984) [Sov. Phys. JETP **59**, 1277 (1984)].
- ¹⁰E. L. Ivchenko and M. M. Sobirov, Fiz. Tverd. Tela (Leningrad) **28**, 2023 (1986) [Sov. Phys. Solid State **28**, 1131 (1986)].
- ¹¹R. L. Weiher and W. C. Tait, Phys. Rev. B **5**, 623 (1972).
- ¹²C. Benoit a la Guillaume, A. Bonnot, and J. M. Debever, Phys. Rev. Lett. **24**, 1235 (1970).
- ¹³V. M. Agranovich and V. L. Ginzburg, *Crystal Optics with Spatial Dispersion and Exciton*, Springer, New York (1984).
- ¹⁴E. L. Ivchenko, A. V. Sel'kin, A. G. Aubakirov, M. I. Sazhin, and N. Kh. Yuldashev, Opt. Spektrosk. **67**, 845 (1989).
- ¹⁵S. I. Pekar', Zh. Eksp. Teor. Fiz. **33**, 1022 (1957) [Sov. Phys. JETP **6**, 785 (1958)]; Zh. Eksp. Teor. Fiz. **34**, 1176 (1958) [Sov. Phys. JETP **7**, 813 (1958)].
- ¹⁶A. B. Pevtsov, S. A. Permogorov, and A. V. Sel'kin, Pis'ma Zh. Eksp. Teor. Fiz. **39**, 261 (1984) [JETP Lett. **39**, 312 (1984)].
- ¹⁷A. B. Pevtsov, S. A. Permogorov, Sh. R. Saifullaev, and A. B. Sel'kin, Fiz. Tverd. Tela (Leningrad) **22**, 2400 (1980) [Sov. Phys. Solid State **22**, 1396 (1980)].
- ¹⁸A. B. Pevtsov and A. V. Sel'kin, Zh. Eksp. Teor. Fiz. **83**, 516 (1982) [Sov. Phys. JETP **56**, 282 (1982)].
- ¹⁹A. B. Pevtsov and A. V. Sel'kin, *Ellipsometry: Theory, Methods, and Applications*. A. B. Rzhanova and L. A. Il'ina eds. Nauka, Novosibirsk, 1987, p. 156.
- ²⁰E. S. Koteles, *Excitons*. E. I. Rashba and M. D. Sturge, Eds. North Holland, Amsterdam (1982), ch. III.
- ²¹N. N. Akhmediev, Zh. Eksp. Teor. Fiz. **79**, 1534 (1980) [Sov. Phys. JETP **52**, 772 (1980)].

Translated by Frank J. Crowne